Docking Studies on $\alpha_v\beta_3$ Integrin Ligands: Pharmacophore Refinement and Implications for Drug Design

Luciana Marinelli,[†] Antonio Lavecchia,[‡] Kay-E. Gottschalk,[†] Ettore Novellino,[‡] and Horst Kessler*[,†]

Institut für Organische Chemie und Biochemie, Technische Universität München, Lichtenbergstrasse 4, D-85747 Garching, Germany, and Dipartimento di Chimica Farmaceutica e Tossicologica, Università di Napoli "Federico II", Via D. Montesano, 49−80131 Napoli, Italy

Received December 20, 2002

Starting from the first crystal structure of the extracellular segment of the $\alpha_v\beta_3$ integrin receptor with a cyclic RGD ligand bound to the active site, structural models for the interactions of known ligands with the $\alpha_v\beta_3$ integrin receptor were generated by automated computational docking. The obtained complexes were evaluated for their consistency with structure−activity relationships and site-directed mutagenesis data. A comparison between the calculated interaction free energies and the experimental biological activities was also made. All the possible interactions of the investigated compounds at the active site and the probable ligand binding conformations provide an improved basis for structure-based rational ligand design. Additionally, our docking results allow a further validation and refinement of the pharmacophore model previously postulated by us.

Introduction

Integrins are large heterodimeric cell surface receptors, which mediate signal transduction through interactions with cellular or extracellular ligands.[1,2] These receptors are composed of one α and one β subunit, both characterized by a large N-terminal extracellular domain, a transmembrane domain, and a short C-terminal intracellular tail. Eighteen α and eight β mammalian subunits are known, which assemble noncovalently into more than 26 different heterodimers.[3] The most common integrin binding sequence is the Arg-Gly-Asp (RGD) motif, found within many extracellular matrix proteins and disintegrins.[4,5] However, different integrins recognize diverse RGD-containing proteins differently. The specificity is attributed to the sequences flanking the RGD triad, the auxiliary binding motifs in the ligand, and to a large extent to the conformational presentation of the triad.[6]

Here, we focus on the $\alpha_v\beta_3$ integrin (vitronectin receptor), which binds various RGD-containing proteins,[7] including fibronectin, fibrinogen, vitronectin, and many disintegrins and small peptides. The $\alpha_v\beta_3$ integrin is expressed on the surface of a variety of cell types, including platelets, endothelial cells, vascular smooth muscle cells, osteoclasts, and tumor cells. This integrin plays a key role in numerous physiological processes such as angiogenesis,[8−10] apoptosis,[11,12] and bone resorption.[13,14]

Ligands[15] of integrin $\alpha_v\beta_3$ are expected to have a major impact on the treatment of several human diseases such as osteoporosis,[16,17] rheumatoid arthritis,[18−20] and cancer.[21−24] One major problem in the design of strong and selective $\alpha_v\beta_3$ integrin ligands in the past has been the lack of detailed structural information on the interaction between $\alpha_v\beta_3$ integrin receptor and its ligands. Until recently, drug design efforts have relied on pharmacophore hypotheses derived from the structures of known ligands. Three pharmacophoric regions have been identified: (i) a carboxylate group, (ii) a guanidinium(-like) moiety, and (iii) a hydrophobic group, the geometrical relationships of which were elucidated.[25,26] Although this pharmacophore model was successful in developing highly potent ligands, many uncertainties remain about the details of the receptor−ligand interaction.

With the appearance of the X-ray structure of the $\alpha_v\beta_3$ integrin headgroup[27] together with the first complex of the $\alpha_v\beta_3$ integrin extracellular segment with an RGD-containing ligand bound to the active site,[28] structure-based rational design of highly active ligands becomes possible. Based on the apo-$\alpha_v\beta_3$ integrin headgroup, molecular modeling studies were performed to identify the binding region and to predict the conformational changes accompanying the ligand binding event.[29,30] A comparison between the modeled protein complex and the experimentally observed one shows that the trend in the β-subunit change has been predicted correctly as well as the position of the metal ion in the MIDAS region while the orientation of the arginine mimetic group in the docked ligand differs from that in the X-ray structure. Recently, manual docking has been carried out using the unbound $\alpha_v\beta_3$ integrin in an effort to elucidate the binding mode of some nonpeptide ligands.[31] However, in contrast with the crystal structure of the ligand−integrin complex, all of the investigated compounds in the latter study do not bind to the metal ion at the MIDAS region, which was assumed to be unoccupied as in the unbound receptor.

Here, we report docking studies of $\alpha_v\beta_3$ ligands using the recently published X-ray complex in order to better understand the ligand−integrin interactions and to define the pharmacophoric requirements of the ligands on a structural basis. The automated molecular docking

* To whom correspondence should be addressed. Tel: +49-89-289 13300. Fax: +49-89-289 13210. E-mail: kessler@ch.tum.de.
[†] Technische Universität München.
[‡] Dipartimento di Chimica Farmaceutica e Tossicologica, Università "Federico II" di Napoli.

10.1021/jm020577m CCC: $25.00
Published on Web 09/10/2003

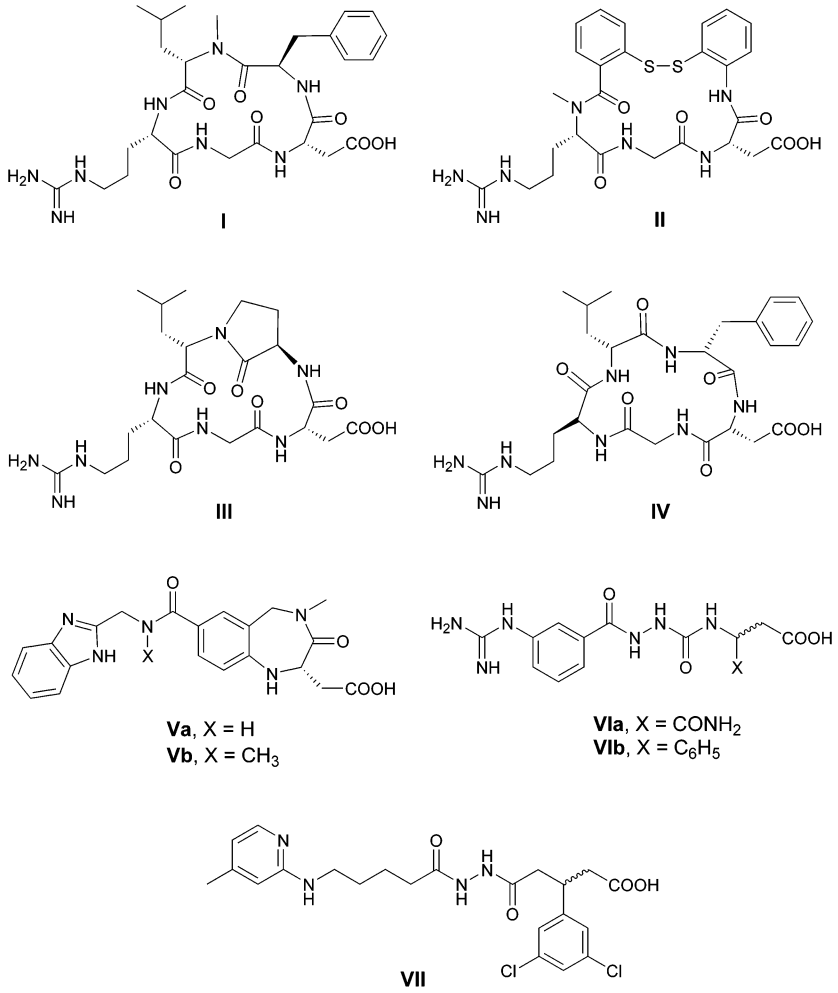

Figure 1. Structures of the investigated ligands.

calculations were carried out using the version 3.0.5 of the AutoDock program, which has been shown to successfully reproduce experimentally observed binding modes.[32,33] While the protein is required to be rigid, the program allows torsional flexibility in the ligand. It combines an energy evaluation through precalculated grids of affinity potentials with a variety of search algorithms to find suitable binding positions for a ligand on a given protein.

For docking experiments, we have chosen peptidic, peptidomimetic, and nonpeptidic compounds with a high molecular diversity and inhibitory potencies ranging from micromolar to nanomolar values. The structures of the investigated ligands are shown in Figure 1.

Extensive ligand-based drug design studies, using cyclic peptide libraries with constrained backbone conformations, led to the discover of the $\alpha_v\beta_3$-selective first-generation cyclic pentapeptide *cyclo*(-RGDfV-).[6,26,34] The systematic derivatization of this peptide[35] resulted in the N-alkylated cyclopeptide *cyclo*(-RGDf[NMe]V-)[36] (**I**, IC_{50} = 0.6 nM), which is in clinical phase II as anticancer drug (Cilengitide, EMD 121974). This is the ligand for which the crystal structure of the complex has been reported. In our study, *cyclo*(-RGDf[NMe]V-) has been used as a reference for the analysis of the other compounds. The semipeptide 2-mercaptobenzoyl-(*N*α-methyl)RGD-2-mercaptoanilide cyclic disulfide (**II**) is an active analogue with a K_i of 3.5 nM, whose structure unbound to an integrin receptor has been solved by X-ray diffraction. [37,38]

Later on, several *turn* mimetics and sugar amino acids were incorporate into the lead structure *cyclo*-(-RGDfV-) by replacing the D-Phe-Val dipeptide unit.[39,40] These investigations led to several potent $\alpha_v\beta_3$ peptidomimetic ligands, among which we have chosen the *cyclo*(-RGD"R-ANC") as a representative compound (**III**, IC_{50} = 0.8 nM)[39] for this study.

A systematic study of all retro-, inverso-, and retro-inverso isomers of the sequence RGDFV yielded the highly active compound *cyclo*(-vfdGR-) (**IV**, IC_{50} = 40 nM).[41] Subsequently, novel nonpeptidic ligands have been designed by several groups.[42−46] Most of them contained an N-terminal guanidino, benzamidino, or aminopyridine group and a carboxyl group separated by a well-defined distance. The introduction of a benzimidazole residue as an arginine mimic resulted in compounds **Va** and **Vb**, which display nanomolar activity toward $\alpha_v\beta_3$ (K_i = 15 nM and K_i = 2 nM, respectively).[47−49] Recently, the highly active compounds **VIa** (IC_{50} = 150 nM), **VIb** (IC_{50} = 2.6 nM), and **VII** (IC_{50} = 6 nM) were derived in our laboratories from RGD-mimetic libraries.[50−52]

The automated docking was performed on this subset of representative ligands. For less active or inactive parent compounds, manual docking was carried out in an attempt to elucidate the reasons behind the reduced

biological activity. Moreover, the correlation between the biological activities of the compounds and calculated ligand−protein interaction energies was investigated.

This is the first study that examines the relationship between the structure and the potency of $\alpha_v\beta_3$ integrin ligands on the level of binding free energy predictions using automated docking algorithm.

Methods

Docking. Docking calculations were performed using version 3.0.5 of the AutoDock program package.[32] Three search methods, Monte Carlo simulated annealing, a traditional genetic algorithm, and the Lamarckian Genetic Algorithm (LGA) are available in AutoDock 3.0.5 It has been shown that the most efficient, reliable, and successful of these methods is the latter.[32]

Thus, docking of ligands **I-VII** to $\alpha_v\beta_3$ integrin was carried out using the provided empirical free energy function and the LGA as implemented in AutoDock program, applying a protocol with an initial population of 50 randomly placed individuals, a maximum number of 1.5×10^6 energy evaluations, a mutation rate of 0.01, a crossover rate of 0.80, and an elitism value of 1. For the local search, the pseudo-Solis and Wets algorithm was applied using a maximum of 300 interactions per local search. Fifty independent docking runs were carried out for each ligand. Results differing by less than 1.5 Å in positional root-mean-square deviation (rmsd) were clustered together and represented by the result with the most favorable free energy of binding. The obtained complexes were energetically minimized using both steepest descent and conjugated gradient algorithms, permitting only the ligand and the side chain atoms of the protein within a radius of 5 Å around the ligand to relax. Energy minimizations were carried out employing the DISCOVER program with the CVFF force field.[59]

Ligand Setup. The structures of the ligands were generated from the standard fragment library of the SYBYL software version 6.8,[53] if no experimental structure was available. Geometry optimizations were achieved with the SYBYL/MAXIMIN2 minimizer by applying the BFGS (Broyden, Fletcher, Goldfarb, and Shannon) algorithm[54] with a convergence criterion of 0.001 kcal/mol and employing the TRIPOS force field.[55] Partial atomic charges were assigned using the semiempirical MOPAC/AM1 method,[56] as implemented in the SYBYL package. In case of the nonpeptidic ligands, all the relevant torsion angles were treated as flexible during the docking process, allowing thus a search of the conformational space. In the compounds **Va** and **Vb**, the various benzodiazepine ring conformations were taken into account. For **VIa** and **VIb**, the Cambridge Structural Database (CSD)[57] was searched to investigate the conformational preference of the diacylhydrazine moiety. Since the torsion angle C−N−N−C was mostly found to be −90°, which is also in accordance to ab initio studies,[58] the geometry of this fragment was held fixed during the calculations. If the configuration of one stereocenter is not reported, both the *S* and the *R* isomers were analyzed, otherwise the published stereochemistry was chosen. For the peptidic and peptidomimetic ligands, the conformations in solution as experimentally determined by NMR and subsequent molecular dynamics (MD) in explicit solvent were used as starting conformation. During the docking process the backbone conformation was held fixed, while the side chain dihedral angles were free to rotate.

Protein Setup. Xiong et al. have recently solved the crystal structure of the extracellular domain of the $\alpha_v\beta_3$ integrin receptor in complex with **I** and in the presence of the proadhesive ion Mn^{2+} (PDB entry code = 1L5G).[28] Since in the X-ray structure the headgroup of $\alpha_v\beta_3$ integrin, which comprises the β propeller domain of α_v and the βA domain of β_3, has been identified as the ligand binding region, the docking was performed only on the globular head. The protein structure was set up for docking as follows: polar hydrogens were added using the BIOPOLYMERS module of the SYBYL program (residues Arg, Lys, Glu, and Asp were considered ionized while all His were considered neutral by default), Kollman united-atom partial charges were assigned, and all waters were removed. Because of the lack of parameters for the Mn^{2+} ions, we modeled them by replacing the Mn^{2+} ions in the experimental protein structure with Ca^{2+} ions. To optimize the side chain and the hydrogen positions, the protein structure was minimized using both steepest descent and conjugate gradient, keeping the backbone atoms constrained. The optimization was carried out employing the DISCOVER program[59] with the CVFF force field. Solvation parameters were added to the final protein file using the ADDSOL utility of the AutoDock program. The grid maps, representing the protein in the docking process, were calculated with AutoGrid. The grids were chosen to be large enough to include a significant part of the protein around the binding site. In all cases, we used grid maps with $61 \times 61 \times 61$ points with a grid-point spacing of 0.375 Å. The center of the grid was set to be coincident with the mass center of the ligand in the crystal complex.

Results

Docking of the compounds **I**−**VII** revealed a consistent set of recurring interactions. An important characteristic of the interaction between all the substrates and the $\alpha_v\beta_3$ integrin receptor is the presence of an extensive network of hydrogen bonds between the ligand and the receptor side chains. The most important interactions found for each compound are summarized in Table 1. Although the predicted free energy of binding is a useful descriptor of ligand−receptor complementarity, the choice of the "best" docking model was ultimately dictated also by its agreement with the structure−activity relationships (SARs) and the site-directed mutagenesis data. Finally, for each ligand a comparison with some less active parent compounds was made. The results are briefly described in the following section.

I. With the aim to test the AutoDock program for its ability to reproduce the crystallized binding geometry of *cyclo*(-RGDf[NMe]V-), as well as for comparative purposes, **I** was subjected to automated docking calculations. The program was successful in reproducing the experimentally found binding mode of **I**, as it corresponds to the most populated cluster and is among the first three solutions (estimated free energy of binding, $E = -8.9$ kcal/mol). Both the X-ray complex and the calculated complex reveal that the cyclic pentapeptide inserts into a crevice between the propeller and the βA domain on the integrin head. The Arg and the Asp side chains of the ligand point to opposite direction. The Arg side chain inserts into a narrow groove at the top of the propeller domain, and its guanidinium group is held in place by a bidentate salt bridge to (α)-Asp218 and by an additional salt bridge to (α)-Asp150. On the opposite side, one of the Asp carboxylate oxygens contacts the metal ion at the MIDAS in βA, while the other carboxylate oxygen forms a hydrogen bond with the backbone amide hydrogen of (β)-Asn215. Furthermore, the backbone NH of Asp is involved in a hydrogen bond with the backbone carbonyl oxygen of (β)-Arg216. The glycine residue lies at the interface between the α and β subunits directly on the surface of the protein, making hydrophobic interactions. Additionally, D-Phe is involved in a T-shaped interaction with (β)-Tyr122. The valine side chain does not seem to interact with the protein at all.[28,30] A schematic representation of the above-described interactions is depicted in Figure 2.

Table 1. Result of 50 Independent Docking Runs for Each Ligand[a]

ligand	N_{tot}	ΔG_{bind}	surrounding residues
I	4	−8.9	**(α)-D150,** (α)-F177, (α)-Y178, (α)-Q180, (α)-T212, (α)-A213, **(α)-D218**, (*β*)-R214, **(*β*)-N215**, **(*β*)-R216**, (*β*)-D217, (*β*)-A218, (*β*)-S121, (*β*)-Y122, (*β*)-S123
II	3	−10.6	**(α)-D150**, (α)-F177, (α)-Y178, **(α)-Q180,** (α)-T212, (α)-A213, **(α)-D218**, (*β*)-R214, **(*β*)-N215**, (*β*)-R216, (*β*)-D217, (*β*)-A218, (*β*)-E220, (*β*)-S121, (*β*)-Y122, (*β*)-S123, (*β*)-D251
III	4	−8.9	(α)-D150, (α)-Y178, **(α)-Q180**, (α)-T212, (α)-A213, (α)-A215, **(α)-D218**, **(*β*)-R214**, **(*β*)-N215**, (*β*)-R216, (*β*)-D217, (*β*)-A218, (*β*)-S121, (*β*)-Y122, (*β*)-S123
IV	3	−8.1	**(α)-D150**, (α)-F177, (α)-Y178, (α)-Q180, (α)-T212, (α)-A213, **(α)-D218**, (*β*)-R214, **(*β*)-N215**, (*β*)-R216, (*β*)-D217, (*β*)-A218, (*β*)-S121, (*β*)-Y122, (*β*)-S123, (*β*)-D251
Va	4	−10.3	(α)-D150, (α)-F177, (α)-Y178, (α)-Q180, (α)-T212, (α)-A213, (α)-A215, **(α)-D218**, **(*β*)-R214**, **(*β*)-N215**, **(*β*)-R216**, (*β*)-D217, (*β*)-A218, (*β*)-S121, (*β*)-Y122, (*β*)-S123, (*β*)-E220
Vb	3	−10.3	(α)-D150, (α)-F177, (α)-Y178, (α)-Q180, (α)-T212, (α)-A213, (α)-A215, **(α)-D218**, **(*β*)-R214**, **(*β*)-N215**, **(*β*)-R216**, (*β*)-D217, (*β*)-A218, (*β*)-S121, (*β*)-Y122, (*β*)-S123, (*β*)-E220
VIa	4	−9.0	**(α)-D150**, (α)-F177, (α)-Y178, (α)-Q180, (α)-A213, **(α)-D218**, **(*β*)-N215**, **(*β*)-R216**, (*β*)-D217, (*β*)-A218, (*β*)-S121, (*β*)-Y122, **(*β*)-S123**, (*β*)-E220, (*β*)-D251, (*β*)-A252
VIb	4	−9.4	**(α)-D150**, (α)-F177, (α)-Y178, (α)-A215, **(α)-D218**, (*β*)-V157, (*β*)-N215, **(*β*)-R216**, (*β*)-D217, (*β*)-A218, (*β*)-S121, (*β*)-Y122, **(*β*)-S123**, (*β*)-D251, (*β*)-A252
VII	4	−9.2	(α)-D150, (α)-F177, (α)-Y178, (α)-Q180, (α)-A215, (α)-D218, (α)-A213, (α)-Q214, (α)-A215, (*β*)-R214, **(*β*)-N215**, (*β*)-R216, (*β*)-D217, (*β*)-A218, (*β*)-S121, (*β*)-Y122, (*β*)-S123, (*β*)-E220, (*β*)-D251.

[a] N_{tot} is the number of conformational clusters; ΔG_{bind} is the estimated free energy of binding for the top cluster results and is given in kcal/mol. The last column shows the residues of the binding site located within 5 Å from any atom of the docked ligands. Residues, which form hydrogen bonds with the ligand are highlighted in bold.

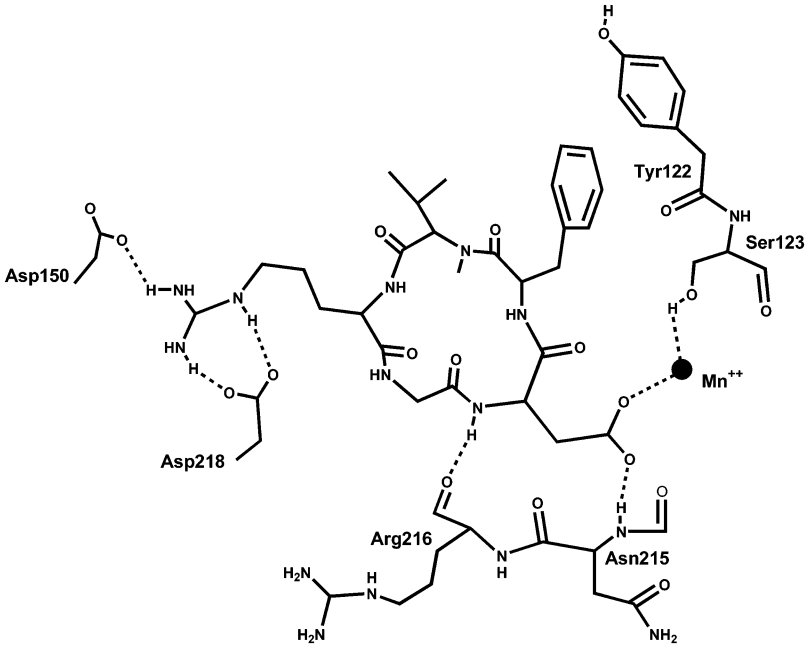

Figure 2. Schematic representation of **I**−$\alpha_v\beta_3$ integrin complex showing the major protein−ligand interactions.

From our docking calculations we found a possible second binding mode, which is less populated in our calculations and has a 2 kcal/mol higher free energy of binding. The difference in respect to the top-ranking binding mode resides in the orientation of the upper part of the ligand, which occupies the region of (α)-Ile216 and (*β*)-Lys253, making some hydrophobic interactions. As the cleft in which the ligand binds is rather shallow and the upper portion of the ligand makes virtually no contact with the protein, a certain ambiguity of the ligand orientation may be possible. In both orientations, it seems as if the Asp and Arg of the RGD ligands act like an electrostatic clamp, attaching to charged regions of the protein.[30]

II. The compound with the lowest free energy of binding (E = −10.6 kcal/mol) is representative of the most populated cluster and strongly resembles the best calculated (and experimentally observed) binding mode of I. As shown in Figure 3, the guanidinium group engages a bidentate salt bridge to the (α)-Asp150 carboxylate group and donates a hydrogen bond to the (α)-Asp 218 and (α)-Gln180 side chains. In the same way as **I**, the Asp carboxylate group coordinates the Ca^{2+} ion and acts as a hydrogen bond acceptor for the backbone NH of (*β*)-Asn215. The aromatic ring next to the Asp residue appears to be oriented such that a T-shaped interaction with the (*β*)-Tyr122 side chain can occur. An alternative binding mode occurs less frequently and with a higher calculated free energy of binding (E = −8.6 kcal/mol) and shows the two aromatic moieties allocated in a large region composed of the following residues: (α)-Ala215, (α)-Ile216, (α)-Agr248, (*β*)-Asp251, (*β*)-Ala252, (*β*)-Lys253.

III. As **III** is a chiral compound, both enantiomers were considered for docking. Notwithstanding the structural similarities at the RGD site, the two analogues reveal different biological activities (RGD"R-ANC", IC_{50} = 0.8 nM and RGD"S-ANC", IC_{50} = 40 nM). The superposition of the two structures, which were determined by NMR spectroscopy and MD simulation in

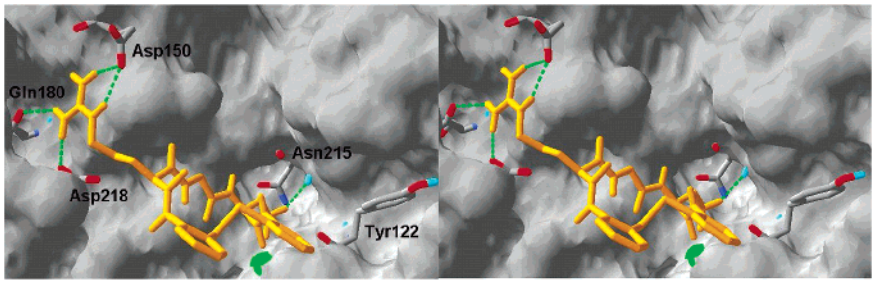

Figure 3. Stereoview showing the binding of compound **II** to $\alpha_v\beta_3$ integrin receptor. The ligand is shown in yellow and the metal ion at the MIDAS region in green. Hydrogen bonds are represented with dashed green lines. Nonpolar hydrogens were removed for clarity.

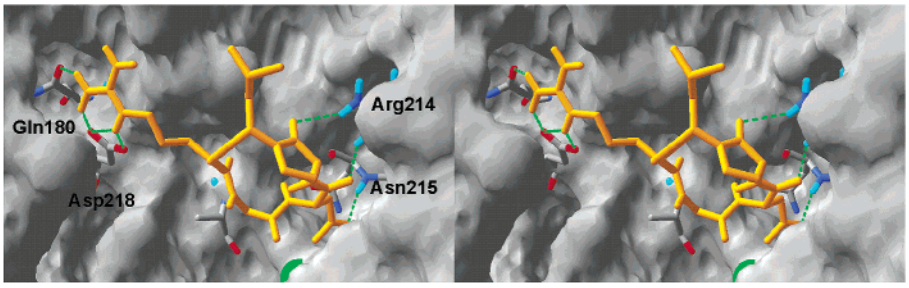

Figure 4. Stereoview showing the binding of compound **III** to $\alpha_v\beta_3$ integrin receptor. Nonpolar hydrogens were removed for clarity.

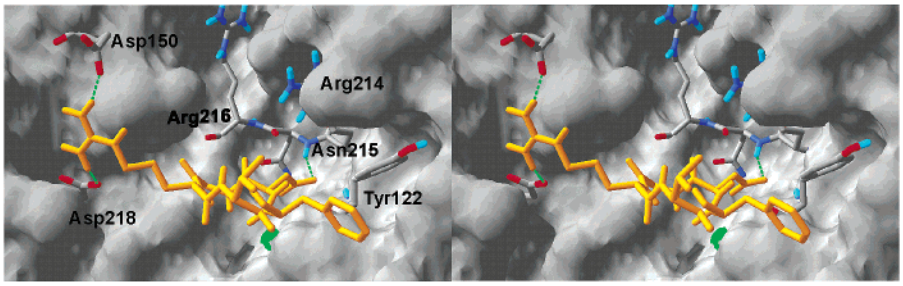

Figure 5. Stereoview showing the binding of compound **IV** to $\alpha_v\beta_3$ integrin receptor. Nonpolar hydrogens were removed for clarity.

water, shows that the S-ANC differs from the R-ANC derivative by a 180° rotation of the lactam bond. Thus, it was postulated that the carbonyl group in the R-ANC motif might interact as hydrogen bond acceptor with the receptor. Automated docking of the R-ANC derivative revealed a preference for a single position in the binding pocket. The ligand is found to be in the same location as **I** in the crystal structure (Figure 4). One of the Asp carboxylate oxygens of the ligand complexes the Ca^{2+} ion at the MIDAS region in βA, while the other forms a hydrogen bond with the backbone NH of (β)-Asn215. The glycine residue lies at the interface between the α and β subunits, making an hydrophobic interaction with (β)-Ala218. The Arg side chain inserts into a groove of the propeller domain forming a bidentate salt bridge to (α)-Asp218 and a hydrogen bond to the carbonyl oxygen of (α)-Gln180 side chain. A hydrogen bond from the guanidinium group of (β)-Arg214 to the backbone CO of Asp in the ligand was observed. The expected hydrogen bond was found between the carbonyl oxygen of the R-ANC moiety and the guanidinium group of (β)-Arg214. For the RGD"R-ANC", a less populated binding mode in which the upper part occupies the region of (α)-Ile216 and (β)-Ala252 was also found. The estimated free energy of binding of this less favored binding mode is raised by 2 kcal/mol.

Manual docking of the (*S*)-enantiomer reveals that a similar interaction is not possible, since the carbonyl group in the S-ANC moiety points inside the cycle of the peptidomimetic compound. Thus, the weaker activity of the (*S*)-enantiomer might be ascribed to the nonproductive orientation of the S-ANC carbonyl group.

Many other rigid building blocks such as the β-turn dipeptide (*S*,*S*)-spiro-Pro-Leu were used to replace the D-Phe-Val dipeptide unit in the lead structure *cyclo*(-RGDfV-). [39] The *cyclo*(RGD"spiro") shows no activity within the limits of the test system. This was somewhat surprising as the region of the RGD sequence is very similar to that in the lead structure *cyclo*(-RGDfV-). In an effort to elucidate the reasons for the inactivity of *cyclo*(RGD"spiro"), manual docking was carried out. The dramatic drop in affinity seems to be related to the steric hindrance of the spiro system in the binding site. We observed a severe clash between the spiro moiety and the (β)-Tyr122 backbone as well as the (β)-Ser123 side chain.

IV. The automated docking calculations of **IV** resulted in the binding mode depicted in Figure 5. The hydrogen bonds from the guanidinium group in the ligand to the carboxylate oxygens of (α)-Asp150 and (α)-Asp218 are conserved. The other vital interaction between the carboxylate group of Asp in the ligand and the Ca^{2+} ion

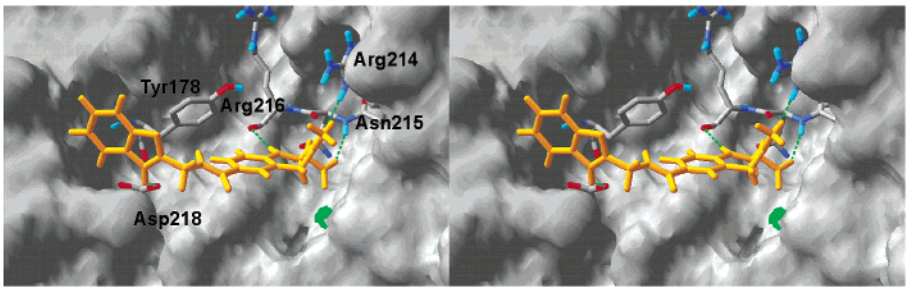

Figure 6. Stereoview showing the binding of compound **Va** to $\alpha_v\beta_3$ integrin receptor.

bound to the MIDAS is preserved as well as the hydrogen bond from one of the carboxylate oxygens to the backbone NH of (β)-Asn215. The phenyl ring is oriented in a such a way that a T-shaped interaction with the aromatic side chain of (β)-Tyr122 is possible. The distance between the centroids of the two rings is 4.3 Å. In the case of **IV**, in which all the peptide bonds have an inverted orientation with respect to **I**, the hydrogen bond between the Asp NH in the ligand and the backbone CO of (β)-Arg216 found in the X-ray complex was not observed for the peptide **IV**.

Manual superposition of the inactive peptide *cyclo*-(-VfdGr-)[41] on both the solution and the crystallized conformation of **I**, as well as on solution structure of **IV**, reveals a slight difference in the position of Asp C^α and a strong difference in the orientation of the $C^\alpha-C^\beta$ vector in the Asp residue. Manual docking as well as automated docking calculations show that the orientation of the $C^\alpha-C^\beta$ vector in the Asp residue of *cyclo*-(-VfdGr-) does not allow a coordination with the metal ion at the MIDAS region. In the case of *cyclo*(-VfdGr-), the automated docking calculations did not converge to a highly populated cluster. It seems as if the *cyclo*-(-VfdGr-) is not able to find a stable position in the binding site. Given these considerations, we believe that a incorrect orientation of the vector $C^\alpha-C^\beta$ in the Asp residue is the reason for the inactivity of *cyclo*(-VfdGr-). However, a more extensive study has to be carried out in order to confirm our hypothesis.

Va and Vb. Prior to the publication of the X-ray structure of the ligand−integrin complex, docking calculations were performed with the compound **Va** starting from the crystal structure of the unbound integrin.[29] While the interactions of the acidic moiety of **Va** turned out to be the same in the modeled complex and in the recently reported X-ray complex, in the earlier docking calculations the arginine mimetic moiety of the ligand bound in the region of (α)-Asp148 and (α)-Tyr178 instead of in the region of (α)-Asp150 and (α)-Asp218 in the α_v propeller domain. Here, using the crystal structure of the $\alpha_v\beta_3$ in the bound conformation, the same ligand was subjected to 50 docking runs as described in Methods. The docking of **Va** reveals that the equatorial benzodiazepine ring conformation enables a favorable interaction with the receptor, while the axial ring conformation prevents the ligand from complexing the Ca^{2+} ion. For the equatorial conformation, a clear preference for one single binding mode is observed. The first top 30 structures are placed similarly to **I** in the crystal complex and show comparable interactions as shown in Figure 6. The benzodiazepine ring lies at the interface between the α and β subunits and forms the center of an extensive network of polar interactions. One of the carboxylate oxygens forms an hydrogen bond with the backbone NH of (β)-Asn215, while the second oxygen coordinates the Ca^{2+} ion at the MIDAS region in βA. The position of the benzodiazepine ring is further stabilized by an hydrogen bond between the carbonyl oxygen in the seven-membered ring and the (β)-Arg214 side chain, and by an additional hydrogen bond between the NH in the benzodiazepine ring and the backbone CO of the (β)-Arg216. As observed for **I**, the guanidine-like functional group inserts in the groove at the top of the propeller domain donating a hydrogen bond to the (α)-Asp218 side chain (another less favorable cluster is present in which the benzimidazole ring is rotated ca. 150°, allowing the formation of an hydrogen bond with the (α)-Asp150 side chain). Furthermore, the benzimidazole ring give rises to a T-shaped interaction with the (α)-Tyr178 aromatic ring. The difference in results between the new and the old docking calculations is due to the use of the unbound integrin receptor.[29] In the unbound $\alpha_v\beta_3$ integrin, the (α)-Asp150 side chain does not point toward the active site, and the position of the (α)-Asp218 is modified compared with the bound conformation of the same integrin. Moreover, the orientation of the (α)-Tyr178 in the unbound receptor does not allow a favorable accommodation of the arginine mimetic group in the groove at the top of the propeller domain.

By looking at the benzodiazepine series synthesized so far, it is interesting to note that the amide *N*-methylation in the compound **Va** (K_i =15 nM) resulted in an increase in activity (**Vb**, K_i = 2 nM).[47] The higher affinity of the methylated compound could be, in principle, ascribed to additional hydrophobic interactions of the methyl group or, alternatively, to the stabilization of the benzimidazole ring in the correct position. To gain more insight into this feature, we performed docking studies on the methylated compound **Vb**. From a careful examination of the resulted complex, no additional hydrophobic interactions were found. Therefore, we believe that the insertion of the methyl obliges the benzimidazole ring to adopt the correct orientation. However, the AutoDock program was not able to reproduce the slight difference in activity, since the methylated ligand has a calculated free energy of binding equal to that of the nonmethylated compound (see Table 1).

In addition to the mentioned studies, *m*- and *p*-benzamidine derivatives were synthesized as arginine-mimetic.[47] The *p*-benzamidine derivative has a K_i of 56 μM, while the meta derivative has a K_i of 0.5 μM. Manual docking of the para derivative reveals that the arginine-mimetic portion is not properly oriented, as the amidine terminus points outside the receptor surface.

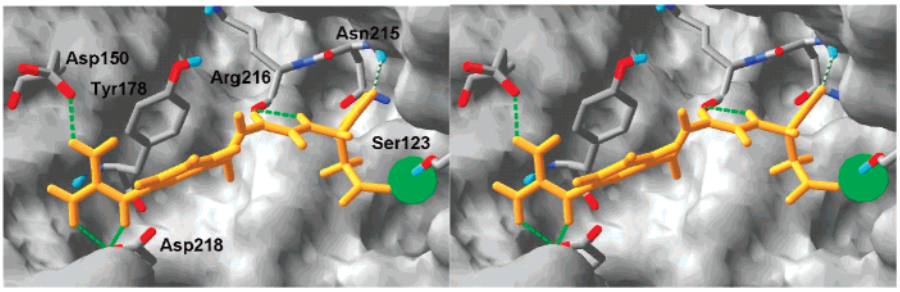

Figure 7. Stereoview showing the binding of compound **VIa** to $\alpha_v\beta_3$ integrin receptor.

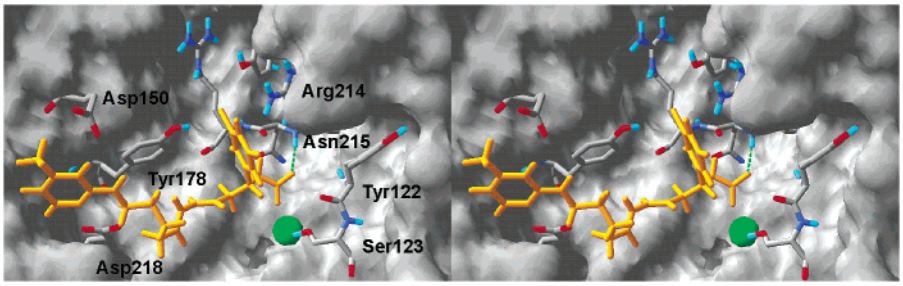

Figure 8. Stereoview showing the binding of compound **VII** to avb3 integrin receptor.

In the case of the *m*-benzamidine derivative, the amidine terminus inserts partially into the protein groove enabling some hydrogen bonds. Furthermore, it has been found that exclusively the *S*-enantiomer is active, which demonstrates once more that not only the distances between the carboxylate moiety and the remaining pharmacophoric points are important, but also the correct relative orientation of them.

VIa and VIb. For compound **VIa**, both *S*- and *R*-enantiomers were synthesized and their potencies were evaluated.[51] Since the *S*-enantiomer exhibited a higher affinity to the $\alpha_v\beta_3$ receptor ($IC_{50} = 150$ nM) than the respective *R*-enantiomer ($IC_{50} = 7200$ nM), only the first one was subjected to the automatic docking calculation. Just like **I** and most of the compounds here docked, **VIa** locates in the center of the typical binding pocket and shares common binding features.

As illustrated in Figure 7, the carboxylate group coordinates the Ca^{2+} at the MIDAS region and, at the same time, is involved in a hydrogen bond with the (β)-Ser123 side chain. Compared to **I**, the carboxylate groups are not coinciding in space, although they occupy the same pocket and both coordinate the metal ion. A hydrogen bond between the (β)-Asn215 backbone NH and the carbonyl oxygen of the $CONH_2$ group in the ligand was found. Moreover, one NH of the diacylhydrazine moieties together with the NH next to the chiral carbon, both make hydrogen bonds with the backbone CO of (β)-Arg216. In **VIa**, the aromatic spacer appears to be optimally oriented for a π-stacking interaction with the aromatic side chain of (α)-Tyr178. The planes of the two rings are fairly parallel and separated by a distance of 4.1 Å. The guanidinium group of the ligand inserts into the groove at the top of the propeller domain forming hydrogen bonds with the (α)-Asp150 and (α)-Asp218 side chains.

Since the compound **VIb** ($IC_{50} = 2.6$ nM) was synthesized as racemic mixture, both enantiomers were subjected to the automated docking calculations. As occurred for the previously examined compounds, the *R*-enantiomer does not seem to fit properly in the binding region. Because of the structural similarity of **VIb** and **VIa**, the binding mode of **VIb** is found to strongly resemble that found for **VIa**. An interesting feature is the position of the phenyl ring attached to the chiral carbon. It inserts into a well-defined pocket framed by the following residues: (β)-Ser121, (β)-Tyr122, (β)-Ser123, (β)-Val157, (β)-Arg214, (β)-Asn215, and (β)-Arg216. This deep cleft can accommodate the Asp side chain in the peptidic ligands, as well as the phenyl ring in **VIb**.

VII. A binding mode similar to that seen in the crystal structure is also found for compound **VII** (*S*-enantiomer) and is depicted in Figure 8. The most favorable result, which has a free energy of binding of -9.2 kcal/mol, places the pyridine ring of the ligand in the groove at the top of the propeller domain, where also the arginine side chain of **I** is positioned. The carboxylate group was found to align with the accordant group of **I** in the X-ray complex. Thus, the coordination to the Ca^{2+} ion at the MIDAS and the hydrogen bond to the backbone NH of (β)-Asn215 are conserved. The dichloro phenyl ring inserts in a region composed mainly by the following residues: (α)-Tyr178, (β)-Tyr122, (β)-Tyr166, (β)-Arg214, (β)-Asn215, (β)-Arg216. In the top ranking cluster a cation-π interaction between the phenyl ring of the ligand and the (β)-Arg214 guanidinium group is present, while in the second top ranking cluster the phenyl group gives rise to a T-shaped interaction with the (β)-Tyr122 aromatic ring.

Discussion

The docking studies presented here provide a structural basis for a large range of integrin−ligand interactions, which will allow the design of next-generation compounds with enhanced activities. Nevertheless, the consistency of our models needs first to be critically assessed. However, at first glance, the docking results seem to be self-consistent, as the functional groups of similar chemical character are placed in similar ways for all docked ligands and show comparable interactions with the protein. Furthermore, the agreement between

the calculated interaction free energies and the experimental determined activities together with the reported SAR studies suggest that the binding modes of the examined ligands are reasonable.

Comparison between the Estimated Binding Free Energy and the Biological Activity. The chosen subset of compounds was used to derive a relationship between experimental values of IC_{50} or K_i and the values predicted by the AutoDock program. On the basis of the traditional molecular force field model of interaction, a new free energy binding score function, which comprises the desolvation upon binding, was derived and adopted in AutoDock.[32] The new free energy of binding E as estimated with the AutoDock program compare reasonably well with the experimental inhibition data. The estimated K_i values for **II**, **Va**, and **Vb** are in the nanomolar range as reported in the literature. The compound **VIb** ($IC_{50} = 2.6$ nM) was found to have a lower estimated K_i as compared to **VIa** ($IC_{50} = 150$ nM) and **VII** ($IC_{50} = 6$ nM). Within a series of structurally related compounds as in the case of **VIa** and **VIb**, the program was able to determine the more active compound, since the E as well as the calculated K_i are lower for **VIb**. However, a comparison beyond these general considerations is not feasible as the IC_{50} and K_i values are not directly comparable, and the experimental data were determined by different methods. Moreover, the new energy function is reported to have a residual standard error of about 2 kcal/mol, which precludes a detailed comparison. Nevertheless, this is a good performance for an empirical free energy function, as it allows a rather accurate estimation of the affinity range as reported in the literature.

Validation of the Binding Models on the Basis of SARs and Mutagenesis Data. In accordance with the SAR studies made on cyclic peptides,[25,26,34−36,39−41] the Asp and Arg side chains point in opposite direction and are separated by a defined distance. The present study together with the recent published X-ray complex indicate that the occasionally postulated salt bridge between the arginine and the aspartate side chain in the solution conformation of the RGD-containing peptides[60,61] is not compatible with the bioactive conformation.

We believe that a proper distance between the arginine and the aspartate group together with the correct orientation of them is necessary to bind both the α and the β subunits simultaneously. Indeed, substitution of Arg by Lys or Asp by Glu in the lead compound *cyclo*-(-RGDfV-) destroys the $\alpha_v\beta_3$ binding activity.

Furthermore, SAR studies show that in **I** the replacement of Gly by Ala or any other amino acid leads to a dramatic drop in activity. This finding is consistent with our complexes, in which a tight receptor binding occurs. The methyl group of Ala residue or any other substituents on that position prevents a close contact with the protein surface by repulsive interactions with receptor residues. In addition, the SAR investigations demonstrate that a hydrophobic aromatic amino acid next to the Asp increases the activity for the $\alpha_v\beta_3$ receptor. Thus, substitution of D-Phe by D-Trp or βNal increases the binding affinity, while D-Pro or D-Tic abolishes the activity. Superposition of the NMR structures of the D-Phe, D-Pro or D-Tic containing peptides with the docked ligands in the binding site, reveals that the D-Trp enlarges the hydrophobic interaction with the (β)-Tyr 122, while the D-Pro or D-Tic containing peptides cannot attach to the protein in a similar way without creating clashes between the D-amino acid side chains and the integrin surface.[30] Moreover, screening of different residues at the Val position of the lead *cyclo*(-RGDfV-) compound demonstrate that this amino acid can be replaced by many different moieties of variable size.[39] This is in complete accordance with our models, in which the part corresponding to the Val side chain in *cyclo*-(-RGDfV-) does not make any contacts to the protein.

Regarding the benzodiazepine compounds **Va** and **Vb**, the SARs clearly indicate the importance of a free NH group in the guanidinium mimetic moiety, since methylation of the benzimidazole nitrogen cause a drop in activity, as does a substitution of benzimidazole ring with a benzoxazole or a benzothiazole ring.[48] This finding is in agreement with the pharmacophoric role assigned to this NH as it donates a hydrogen bond to the (α)-Asp218 side chain in our complex-models. Furthermore, substitution of benzimidazole system with an indole ring led to a loss of activity, indicating that a fused ring is important. A detailed analysis of our docking results reveals a T-shaped interaction between the aromatic ring in the arginine mimetic chain and the (α)-Tyr 178 phenyl ring. Furthermore, the (β)-Asn 215 that is found to donate a hydrogen bond to one of the carboxylate oxygens of all the ligands examined here has recently identified as a critical residue for ligand binding by site-directed mutagenesis.[62]

SARs relative to the recently synthesized RGD mimetic libraries are now reconsidered in the light of the binding models for compound **VIa**, **VIb**, and **VII**.[50−52] SARs studies clearly indicate that the replacement of the $CONH_2$ group in **VIa** with an aromatic moiety (**VIb**) has a favorable impact on the activity to the vitronectin receptor. This finding is in accordance with the favorable accommodation of the phenyl ring in **VIb** in a pocket made up by residues (α)-Tyr178, (β)-Tyr122, (β)-Tyr166, (β)-Arg214, (β)-Asn215, and (β)-Arg216. This region has been proposed as a probable ligand binding site on the basis of site-direct mutagenesis studies, performed with naturally occurring β_3 mutants as well as photoaffinity cross-linking experiments.[62−64]

Furthermore, it has been demonstrated that in the aryl guanidine series exchanging the meta-substituted aromatic spacer with an alkyl chain leads to a drop in activity.[50] Our docking results reveal a π-stacking interaction between the aromatic spacer in **VIa** and **VIb** and the side chain of (α)-Tyr178. It is worth noting that mutation of (α)-Tyr 178 to alanine in α_v abolishes fibrinogen binding.[64] In contrast, the pentanoic acid spacer in conjunction with the 2-aminopyridine leads to the highly active compound **VII**. The best combinations between the spacers and the basic groups seems to be the arylguanidine and the alkylaminopyridine.[50] The reason might be the nonplanarity of the pyridine-benzene system, which prevents the optimal spatial orientation of the pharmacophoric basic group.

Our binding models and the mutagenesis data are mutually consistent and collectively provide indications on which interactions in the binding pocket might be responsible for the variance in biological activity and

which additional interactions may be taken into account in the design of new ligands.

Recently, theoretical models of some non-peptide $\alpha_v\beta_3$ ligands in complex with the integrin have been reported by Feuston et al.[31] These authors have performed manual docking studies using the crystal structure of the extracellular domain of the unbound $\alpha_v\beta_3$ integrin receptor. Although a direct comparison is not feasible as the investigated compounds are different from ours, a visual inspection of the reported complexes suggests that the proposed binding models are different from that presented by us. Specifically, all the ligands examined by Feuston et al. have the carboxylic acid interacting with (*β*)-Arg214, while in our complexes the carboxylate coordinates the metal ion at the MIDAS region. It has been postulated early on that the Ca^{2+} ion at the MIDAS region of the *β*A domain in the β_3 subunit interacts with the aspartic acid of RGD peptides.[2,63,65] Indeed, such an interaction was recently observed for the *cyclo*(-RGDf-[NMe]V-) in the X-ray complex,[28] and its importance has been recently discussed by Arnaout et al.[66] The difference between our results and that obtained by Feuston et al. is probably due to the fact that in the unbound integrin $\alpha_v\beta_3$, the MIDAS region was not occupied by a metal ion, while in the bound structure used here a metal ion binds in this region, shortening the distance between the ion and the α-subunit and thus enabling the simultaneous interaction of the ligands with the metal ion and the α-subunit.

Pharmacophore Refinement and Guidelines for Structure-Based Ligand Design. The binding site is clearly dominated by polar residues, and the network of the hydrogen bonds between the ligand and the protein residues play a vital role in determining the level of binding affinities for the $\alpha_v\beta_3$ integrin receptor. The challenge for the design of new strong and selective ligands is to make maximum use of the available interaction partners and minimize the conflicts.

Figure 9 shows an overlay of compounds **II**, **III**, **Va**, and **VII** on the experimentally determined $\alpha_v\beta_3$ integrin-bound conformation of **I**. The ligands were superimposed in their putative bioactive conformations by matching the pharmacophoric elements and taking into account their interactions with the $\alpha_v\beta_3$ integrin receptor. In accordance with a previously postulated pharmacophore model,[25,26] three main interaction sites, which consist of an acidic, a basic, and a hydrophobic moiety can be observed. The two main interaction sites in the protein, which may serve as anchors for tight binding active ligands, are given by the metal ion in the MIDAS region (labeled as C in Figure 9) and by (α)-Asp150 and (α)-Asp218 at the top of the propeller domain (labeled as A). Ideally, the interaction with the metal ion is complemented by favorable contacts with the backbone carbonyl oxygen of (*β*)-Arg 216 (labeled as HB1) (cf. **I**, **Va**, **Vb**, **VIa**, **VIb)** as well as with the side chain of (*β*)-Arg214 (labeled as HB2) (cf. the binding models of **III**, **Va**, **Vb**).

Differently, the interaction at the arginine site is complemented by a favorable contact with the (α)-Tyr178 ring (cf. the binding models of **Va**, **Vb**, **VIa**, **VIb)**. The molecular alignment illustrated in Figure 9 suggests the presence of two other sites, a hydrogen bond donor and a hydrogen bond acceptor in the proximity of the carboxylate moiety, which could further refine the $\alpha_v\beta_3$ ligand pharmacophore model. It has been mentioned that the two novel hydrogen bonding groups are not shared by all compounds and therefore have to be considered as accessory. Indeed, compounds based on the 2-benzazepine scaffold, which lack of the hydrogen bonding donor near the carboxylate moiety were found to be highly active on the $\alpha_v\beta_3$ integrin receptor.[49] Additionally, a careful examination of the bound $\alpha_v\beta_3$ integrin structure reveals the presence of a large cleft (region of (α)-Asp148 and (*β*)-Tyr166) adjacent to the pocket in which the carboxylate moiety of the ligand inserts. None of the investigated ligands explores this potential interaction site although the three residues (α)-Glu121, (α)-Asp148, (*β*)-Arg216 appear to be optimally oriented for hydrogen bonds formation.

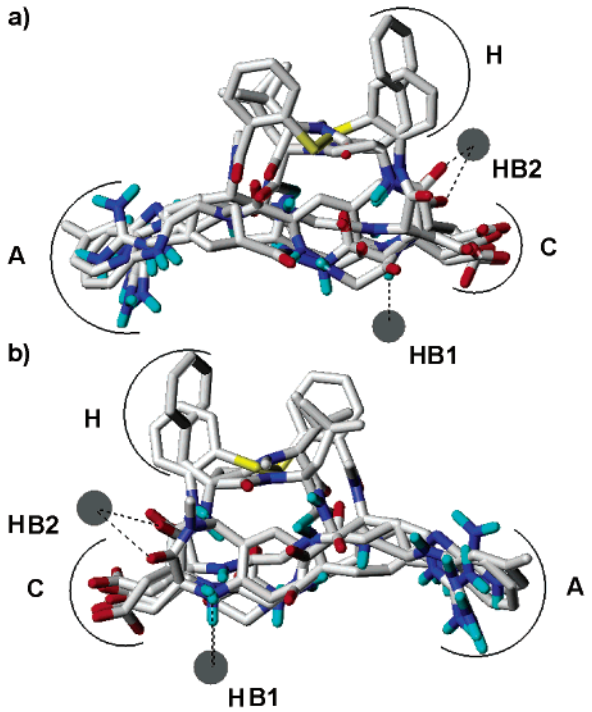

Figure 9. Overlay of putative bioactive conformation of compounds **II**, **III**, **Va**, and **VII** on the experimentally determined $\alpha_v\beta_3$ integrin-bound conformation of **I.** (a, front-side view; b, backside view). The nonpolar hydrogens and the phenyl ring of **VII** are undisplayed for major clarity. A represents the region of (α)-Asp 150 and (α)-Asp 218; C is the MIDAS region in the *β* subunit; H corresponds to (*β*)-Tyr 122, which interacts with the ligands which bear an aromatic ring in the proximity of the carboxylate moiety via a T-shaped interaction; HB1 and HB2 are the proposed novel hydrogen bonding sites (HB1 acceptor and HB2 donor) corresponding to the backbone CO of (*β*)-Arg 216 and the (*β*)-Arg 214 side chain, respectively.

Therefore, the following interactions are hypothesized to govern the ligand−receptor recognition process: (i) coordination of Ca^{2+} ion at the MIDAS from one carboxylate oxygen of the substrate; (ii) a salt bridge between the (α)-Asp218 or the (α)-Asp150 and the guanidine(-like) moiety of the bound ligand; (iii) a T-shaped interaction between the (*β*)-Tyr122 side chain and the aromatic ring of the ligand; (iv) a hydrogen bond donated by one ligand NH to the carbonyl oxygen of (*β*)-Arg216 backbone; (v) a hydrogen bond linking a carbonyl group in the ligand to the (*β*)-Arg214 guanidinium group in the protein. The distances between the phar-

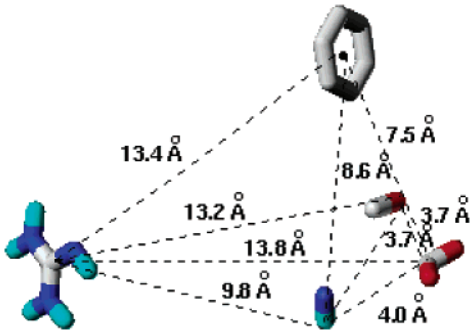

Figure 10. Distances between the pharmacophoric points calculated as an average over the $\alpha_v\beta_3$ integrin-bound conformations of compounds **I**−**VII**. The distances were calculated considering the carbon of the carboxylate moiety, the C^{ζ} of the the guanidinium group or the corresponding atom in the arginine mimetic moieties, the centroid of the aromatic rings, the oxygen of the hydrogen-bonding acceptor group, and the hydrogen of the hydrogen-bonding donor group.

macophoric points calculated as an average over the bound conformations of compounds **I**−**VII** are shown in Figure 10. These distances compare reasonably well with that calculated in our previously proposed three-points pharmacophore model.[25,26]

Conclusion

The recent availability of the X-ray structure of the extracellular segment of integrin $\alpha_v\beta_3$ in complex with an RGD ligand has allowed us to determine the receptor-bound conformations and the mutual alignment of the most representative $\alpha_v\beta_3$ ligands.

A detailed analysis of the interactions between ligands and $\alpha_v\beta_3$ receptors has pointed out which interaction site in the binding pocket might be responsible for the variation in biological activity and which additional interaction can be taken into account for the design of new compounds. Taken together these docking results suggest that an ideal ligand may require a very-well-placed set of polar groups which in turn allow the coordination with the metal ion, the binding to both the (α)-Asp150 and the (α)-Asp218, a polar interaction with the (β)-Arg216 backbone as well as with (β)-Arg214 side chain. The pharmacophore model originally proposed by us has been further validated and refined by the identification of two new hydrogen bonding groups. In conclusion, the result reported here can usefully be employed for the rational design of novel, potent $\alpha_v\beta_3$ ligands in the search for novel anticancer drugs. The next step in this line of research will be the design of lead compounds based on our refined pharmacophore model and on the active site topology.

Acknowledgment. The authors thank Professor Arthur J. Olson for the donation of the Autodock 3.0.5 program. Financial support by the Fonds der Chemischen Industrie is acknowledged.

References

(1) Hynes, R. O. Integrins: Versatility, Modulation, and Signaling in Cell Adhesion. *Cell* **1992**, *69*, 11−25.
(2) Humphries, M. J. Integrin structure. *Biochem. Soc. Trans.* **2000**, *28*, 311−339.
(3) Eble, J. A. *Integrin-Ligand Interaction*; Springer-Verlag: Heidelberg, 1997; pp 1−40.
(4) Ruoslahti, E.; Pierschbacher, M. D. Arg-Gly-Asp- a versatile cell recognition signal. *Cell* **1986**, *44*, 517−518.
(5) D′Souza, S. E.; Ginsberg, M. H.; Plow, E. F. Arginyl-Glycyl-Aspartic acid (RGD) − a cell-adhesion motif. *Trends Biochem. Sci.* **1991**, *16*, 246−250.
(6) Aumailley, M.; Gurrath, M.; Müller, G.; Calvete, J.; Timpl, R.; Kessler, H. Arg-Gly-Asp constrained within cyclic pentapeptides. Strong and selective inhibitors of cell adhesion to vitronectin and laminin fragment P1. *FEBS Lett.* **1991**, *291*, 50−54.
(7) Plow, E. F.; Haas, T. A.; Zhang, L.; Loftus, J.; Smith, J. W. Ligand binding to integrins. *J. Biol. Chem.* **2000**, *275*, 21785−21788.
(8) (a) Brooks, P. C.; Clark, R. A. F.; Cheresh, D. A. Requirement of Vascular integrin $\alpha_v\beta_3$ for Angiogenesis. *Science* **1994**, *264*, 569−571. (b) Ruegg, C.; Dormond, O.; Foletti, A. Suppression of tumor angiogenesis through the inhibition of integrin function and signaling in endothelial cells: which side to target? *Endothelium* **2002**, *9*, 151−160.
(9) Reynolds, L. E.; Wyder, L.; Lively, J. C.; Taverna, D.; Robinson, S. D.; Huang, X.; Sheppard, D.; Hynes, R. O.; Hodivala-Dikle, K. M. Enhanced pathological angiogenesis in mice lacking β3 integrin or β3 and β5 integrins. *Nat. Med.* **2002**, *8*, 27−34.
(10) Hynes, R. O. A reevaluation of integrins as regulators of angiogenesis. *Nature Med.* **2002**, *8*, 918−921.
(11) Montgomery, A. M. P.; Reisfeld, R. A.; Cheresh, D. A. Integrin $\alpha_v\beta_3$ rescues melanoma-cells from apoptosis in 3-dimensional dermal collagen. *Proc. Natl. Acad. Sci. U.S.A.* **1994**, *91*, 8856−8860.
(12) Ruoslahti, E.; Reed, J. C. Anchorage dependence, integrins, and apoptosis. *Cell* **1994**, *77*, 477−478.
(13) Crippes, B. A.; Engleman, V. W.; Settle, S. L.; Delarco, J.; Ornberg, R. L.; Helfrich M. H.; Horton, M. A.; Nickols, G. A. Antibody to β_3 integrin inhibits osteoclast-mediated bone resorption in the thyroparathyroidectomized rat. *Endocrinology* **1996**, *137*, 918−924.
(14) (a) Nakamura, I.; Pilkington, M. F.; Lakkakorpi, P. T.; Lipfert, L.; Sims, S. M. Dixon, S. J.; Rodan, G. A.; Duong, L. T. Role of $\alpha_v\beta_3$ integrin in osteoclast migration and formation of the sealing zone. *J. Cell. Sci.* **1999**, *112*, 3985−3993. (b) Kantlehner, M.; Schaffner, P.; Finsinger, D.; Meyer, J.; Jonczyk, A.; Diefenbach, B.; Nies, B.; Hölzemann, G.; Goodman, S. L.; Kessler, H. Surface coating with cyclic RGD peptides stimulates osteoblast adhesion and proliferation as well as bone formation. *ChemBioChem* **2000**, *1*, 107−114.
(15) Recently, a reevaluation of integrins as regulators of angiogenesis has been reported.[10] The hypothesis that the $\alpha_v\beta_3$ integrin is a negative regulator of angiogenesis is suggested and as a consequence, the drugs targeting it should be considered as agonists rather than antagonists. Although this hypothesis does not dispute the therapeutic potential of the compounds examined here, we will now use the term "ligand" instead of "agonist" or "antagonist".
(16) Chorev, M.; Dresnerpollack, R.; Eshel, Y.; Rosenblatt, M. Approach to discovering novel therapeutic agents for osteoporosis based on integrin receptor blockade. *Biopolymers* **1995**, *37*, 367−375.
(17) Engleman, V. W.; Nickols, G. A.; Ross, F. P.; Horton, M. A.; Griggs, D. W.; Settle, S. L.; Ruminski, P. G.; Teitelbaum, S. L. A peptidomimetic antagonist of the $\alpha_v\beta_3$ integrin inhibits bone-resorption in vitro and prevents osteoporosis in vivo. *J. Clin. Invest.* **1997**, *99*, 2284−2292.
(18) Storgard, C. M.; Stupack, D. G.; Jonczyk, A.; Goodman, S. L.; Fox, R. I. Cheresh, D. A. Decreased angiogenesis and arthritic disease in rabbits treated with $\alpha_v\beta_3$ antagonist. *J. Clin. Invest.* **1999**, *103*, 47−54.
(19) Seemayer, C. A.; Distler, O.; Kuchen, S.; Muller-Ladner, U.; Michel, B. A.; Neidhart, M.; Gray, R. E.; Gray, S. Rheumatoid arthritis: new developments in the pathogenesis with special reference to synovial fibroblasts. *Z. Rheumatol.* **2001**, *60*, 309−318.
(20) (a) Wilder, R. L. Integrin $\alpha_v\beta_3$ as a target for treatment of rheumatoid arthritis and related rheumatic diseases. *Ann. Rheum. Dis.* **2002**, *61 Suppl. 2*, ii96−99. (b) Goligorsky, M. S.; Noiri, E.; Kessler, H.; Romanov, V. Therapeutic potential of RGD peptides in acute renal injury. *Kidney Int.* **1997**, *51*, 1487−1492.
(21) Yun, Z.; Menter, D. G.; Nicolson, G. L. Involvement of integrin $\alpha_v\beta_3$ in cell adhesion, motility, and liver metastasis of murine RAW117 large cell lymphoma. *Cancer Res.* **1996**, *56*, 3103−3111.
(22) Rader, C.; Popkov, M.; Neves, J. A.; Barbas, C. F. 3rd. Integrin $\alpha_v\beta_3$-targeted therapy for Kaposi's sarcoma with an in vitro-evolved antibody. *Faseb. J.* **2002**, *18*, 18.
(23) Trikha, M.; Timar, J.; Zacharek, A.; Nemeth, J. A.; Cai, Y.; Dome, B.; Somlai, B.; Raso, E.; Ladanyi, A.; Honn, K. V. Role for beta3 integrins in human melanoma growth and survival. *Int. J. Cancer* **2002**, *101*, 156−167.

(24) Cooper, C. R.; Chay, C. H.; Pienta, K. J. The role of $\alpha_v\beta_3$ in prostate cancer progression. *Neoplasia* **2002**, *4*, 191−194.
(25) Haubner, R.; Gratias, R.; Diefenbach, B.; Goodman, S. L.; Jonczyk, A.; Kessler, H. Structural and Functional Aspects of RGD-Containing Cyclic Pentapeptides as Highly Potent and Selective Integrin $\alpha_v\beta_3$ Antagonists. *J. Am. Chem. Soc.* **1996**, *118*, 7461−7472.
(26) Pfaff, M.; Tangemann, K.; Müller, B.; Gurrath, M.; Müller, G.; Kessler, H.; Timpl, R.; Engel, J. Selective recognition of cyclic RGD peptides of NMR defined conformation by $\alpha_{IIb}\beta_3$, $\alpha_v\beta_3$ and $\alpha_5\beta_1$ integrins. *J. Biol. Chem.* **1994**, *269*, 20233−20238.
(27) Xiong, J.-P.; Stehle, T.; Diefenbach, B.; Zhang, R.; Dunker, R.; Scott, D. L.; Joachimiak, A.; Goodman, S. L.; Arnaout, M. A. Crystal Structure of the Extracellular Segment of Integrin $\alpha_v\beta_3$. *Science* **2001**, *294*, 339−345.
(28) Xiong, J.-P.; Stehle, T.; Zhang, R.; Joachimiak, A.; Frech, M.; Goodman, S. L.; Arnaout, M. A. Crystal Structure of the Extracellular Segment of Integrin $\alpha_v\beta_3$ in Complex with an Arg-Gly-Asp Ligand. *Science* **2002**, *296*, 151−155.
(29) Gottschalk, K.-E.; Günther, R.; Kessler, H. A Three-State Mechanism of Integrin Activation and Signal Transduction for Integrin $\alpha_v\beta_3$. *ChemBioChem* **2002**, *3*, 470−473.
(30) Gottschalk, K.-E.; Kessler, H. The Structures of Integrins and Integrin-Ligand Complexes: Implications for Drug Design and Signal Transduction. *Angew. Chem., Int. Ed.* **2002**, *41*, 3767−3774.
(31) Feuston, B. P.; Culberson, J. C.; Duggan M. E.; Hartman, G. D.; Leu, C.-T.; Rodan S. B. Binding Model for Nonpeptide Antagonists of $\alpha_v\beta_3$ Integrin. *J. Med. Chem.* **2002**, *45*, 5640−5648.
(32) Morris, G. M.; Goodsell, D. S.; Halliday, R. S.; Huey, R.; Hart, W. E.; Belew, R. K.; Olson, A. J. Automated docking using a Lamarckian genetic algorithm and an empirical binding free energy function. *J. Comput. Chem.* **1998**, *19*, 1639−1662.
(33) Goodsell, D. S.; Morris, G. M.; Olson, A. J. Automated docking of flexible ligands: applications of AutoDock. *J. Mol. Recognit.* **1996**, *9*, 1-5.
(34) Gurrath, M.; Müller, G.; Kessler, H.; Aumailley, M.; Timpl, R. Conformation/activity studies of rationally designed potent anti-adhesive RGD peptides. *Eur. J. Biochem.* **1992**, *210*, 911−921.
(35) Haubner, R.; Finsinger, D.; Kessler, H. Stereoisomeric Peptide Libraries and Peptidomimetics for Designing Selective Inhibitors of the $\alpha_v\beta_3$ Integrin for a New Cancer Therapy. *Angew. Chem., Int. Ed.* **1997**, *36*, 1374−1389.
(36) Dechantsreiter, M. A.; Planker, E.; Mathä, B.; Lohof, E.; Hölzemann, G.; Jonczyk, A.; Goodman, S. L.; Kessler, H. *N*-Methylated Cyclic RGD Peptides as Highly Active and Selective $\alpha_v\beta_3$ Integrin Antagonists. *J. Med. Chem.* **1999**, *42*, 3033−3040.
(37) Peishoff, C. E.; Ali, F. E.; Bean, J. W.; Calvo, R.; D'Ambrosio, C. A.; Eggleston, D. S.; Hwang, S. M.; Kline, T. P.; Koster P. F.; Nichols, A.; Powers, D.; Romoff, T.; Samanen, J. M.; Stadel, J.; Vasko, J.; Kopple, K. D. Investigation of conformational specificity at GPIIb/IIIa: evaluation of conformationally constrained RGD peptides. *J. Med. Chem.* **1992**, *35*, 3962−3969.
(38) Kopple, K. D.; Baures, P. W.; Bean, J. W.; D'Ambrosio, C. A.; Hughes, J. L.; Peishoff, C. E.; Eggleston, D. S. Conformations of Arg-Gly-Asp Containing Heterodetic Cyclic Peptides: Solution and Crystal Studies. *J. Am. Chem. Soc.* **1992**, *114*, 9615−9623.
(39) (a) Haubner, R.; Schmitt, W.; Hölzemann, G.; Goodman, S. L.; Jonczyk, A.; Kessler, H. Cyclic RGD Peptides Containing β-Turn Mimetics. *J. Am. Chem. Soc.* **1996**, *118*, 7881−7891. (b) Belvisi, L.; Bernardi, A.; Checchia, A.; Manzoni, L.; Potenza, D.; Scolastico, C.; Castorina, M.; Cupelli, A.; Giannini, G.; Carminati, P.; Pisano, C. Potent integrin antagonists from a small library of RGD-including cyclic pseudopeptides. *Org. Lett.* **2001**, *3*, 1001−1004.
(40) (a) Lohof, E.; Planker, E.; Mang, C.; Burkhart, F.; Dechantsreiter, M. A.; Haubner, R.; Wester, H. J.; Schwaiger, M.; Hölzemann, G.; Goodman, S. L.; Kessler, H. Carbohydrate Derivatives for Use in Drug Design: Cyclic α_v-Selective RGD Peptides. *Angew. Chem., Int. Ed.* **2000**, *39*, 2761−2764. (b) Sukopp, M.; Marinelli, L.; Heller, M.; Brandl, T.; Goodman, S. L.; Hoffmann, R. W.; Kessler, H. Designed Beta-turn Mimic based on the Allylic Strain Concept: Evaluation of Structural and Biological Features by Incorporation into a Cyclic RGD-Peptide. *Helv. Chim. Acta* **2002**, 85, 4442−4452.
(41) Wermuth, J.; Goodman, S. L.; Jonczyk, A.; Kessler, H. Stereoisomerism and Biological Activity of the Selective and Superactive $\alpha_v\beta_3$ Integrin Inhibitor cyclo(-RGDfV-) and Its Retro-Inverso Peptide. *J. Am. Chem. Soc.* **1997**, *119*, 1328−1335.
(42) Pitts, W. J.; Wityak, J.; Smallheer, J. M.; Tobin, A. E.; Jetter, J. W.; Buynitsky, J. S.; Harlow, P. P.; Solomon, K. A.; Corjay, M. H.; Mousa, S. A.; Wexler, R. R.; Jadhav, P. K. Isoxazolines as Potent Antagonists of the Integrin $\alpha_v\beta_3$. *J. Med. Chem.* **2000**, *43*, 27−40.
(43) Meissner, R. S.; Perkins, J. J.; Duong L. T.; Hartman, G. D.; Hoffman, W. F.; Huff, J. R.; Ihle, N. C.; Leu, C.-T.; Nagy, R. M.; Naylor-Olsen, A.; Rodan, G. A.; Whitman, D. B.; Wesolowski, G. A.; Duggan, M. E. Nonpeptide $\alpha_v\beta_3$ antagonists. Part 2: constrained glycyl amides derived from the RGD tripeptide. *Bioorg. Med. Chem. Lett.* **2002**, *12*, 25−29.
(44) Duggan, M. E.; Duong, L. T.; Fisher, J. E.; Hamill, T. G.; Hoffman, W. F.; Huff, J. R.; Ihle, N. C.; Leu, C.-T.; Nagy, R. M.; Perkins, J. J.; Rodan, S. B.; Wesolowski, G. A.; Whitman, D. B.; Zartman, A. E.; Rodan, G. A.; Hartman, G. D. Nonpeptide $\alpha_v\beta_3$ Antagonists. 1. Transformation of a Potent, Integrin-Selective $\alpha_{IIb}\beta_3$ Antagonist into a Potent $\alpha_v\beta_3$ Antagonist. *J. Med. Chem.* **2000**, *43*, 3736−3745.
(45) Batt, D. G.; Petraitis, J. J.; Houghton, G. C.; Modi, D. P.; Cain, G. A.; Coryay, M. H.; Mousa, S. A.; Bouchard, P. J.; Forsythe, M. S.; Harlow, P. P.; Barbera, F. A.; Spitz, S. M.; Wexler, R. R.; Jadav, P. K.; Disubstituted indazoles as potent antagonists of the integrin $\alpha_v\beta_3$. *J. Med. Chem.* **2000**, *43*, 41−58.
(46) Nicolaou, K. C.; Trujillo, J. T.; Janderleit, B.; Chibale, K.; Rosenfeld, M.; Diefenbach, B.; Cheresh, D. A.; Goodman, S. L. Design, synthesis and biological evaluation of nonpeptide integrin antagonists. *Bioorg. Med. Chem.* **1998**, *6*, 1185−1208.
(47) Keenan, R. M.; Miller, W. H.; Kwon, C.; Ali, F. E.; Callahan, J. F.; Calvo, R. R.; Hwang, S.-M.; Kopple, K. D.; Peishoff, C. E.; Samanen, J. M.; Wong, S. A.; Yuan, C.-K.; Huffman W. F. Discovery of Potent Nonpeptide Vitronectin Receptor ($\alpha_v\beta_3$) Antagonists. *J. Med. Chem.* **1997**, *40*, 2289−2292.
(48) Keenan, R. M.; Miller, W. H.; Lago, M. A.; Ali, F. E.; Bondinell, W. E. Callahan, J. F.; Calvo, R. R.; Cousins, R. D.; Hwang, S.-M.; Jakas, D. R.; Ku, T. W.; Kwon, C.; Nguyen, T. T.; Reader, V. A.; Rieman, D. J.; Ross, S. T.; Takata, D. T.; Uzinskas, I. N.; Yan, C. C. K.; Smith, B. R. Benzimidazole derivatives as arginine mimetics in 1,4-benzodiazepine nonpeptide vitronectin receptor ($\alpha_v\beta_3$) antagonists. *Bioorg. Med. Chem. Lett.* **1998**, *8*, 3165−3170.
(49) Miller, W. H.; Alberts, D. P.; Callahan, P. K.; Calvo, R. R.; Cousins, R. D.; Erhard, K. F.; Heerding, D. A.; Keenan, R. M.; Kwon, C.; Manley, P.; Newlander, A. K.; Ross, S. T.; Samanen, J. M.; Uzinskas, I. N.; Venslavsky, J. W.; Yuan, C.-K.; Haltiwanger, R. C.; Gowen, M.; Hwang, S.-M.; James, I. E.; Lark, M. W.; Rieman, D. J.; Stroup, G. B.; Smith, B. R.; Ward, K. W.; Johanson, K. O.; Huffman, W. Discovery of orally active nonpeptide vitronectin antagonists based on a 2-Benzazepine Gly-Asp mimetic. *J. Med. Chem.* **2000**, *43*, 22−26.
(50) Sulyok, G. A. G.; Gibson, C.; Goodman, S. L.; Hölzemann, G.; Wiesner, M.; Kessler, H. Solid-Phase Synthesis of a Nonpeptide RGD Mimetic Library: New Selective $\alpha_v\beta_3$ Integrin Antagonists. *J. Med. Chem.* **2001**, *44*, 1938−1950.
(51) Gibson, C.; Sulyok, G. A. G.; Hahn, D.; Goodman, S. L.; Hölzemann, G.; Kessler, H. Nonpeptidic $\alpha_v\beta_3$ Integrin Antagonist libraries: On-Bead Screening and Mass Spectrometric Identification without Tagging. *Angew. Chem., Int. Ed.* **2001**, *40*, 165−169.
(52) Goodman, S. L.; Hölzemann, G.; Sulyok, G. A. G.; Kessler, H. Nanomolar Small Molecule Inhibitors for $\alpha_v\beta_6$, $\alpha_v\beta_5$ and $\alpha_v\beta_3$ Integrins. *J. Med. Chem.* **2002**, *45*, 1045−1051.
(53) SYBYL Molecular Modeling System (version 6.8), TRIPOS Assoc., St. Louis, MO.
(54) Head, J.; Zerner, M. C. A Broyden-Fletcher-Goldfarb-Shanno Optimization Procedure for Molecular Geometries. *Chem. Phys. Lett.* **1985**, *122*, 264−274.
(55) Vinter, J. G.; Davis, A.; Saunders: M. R. Strategic Approaches to Drug Design. 1. An Integrated Software Framework for Molecular Modelling. *J. Comput.-Aided Mol. Design* **1987**, *1*, 31−55.
(56) (a) MOPAC (version 6.0) is available from Quantum Chemistry Program Exchange, No. 455. (b) Dewar, M. J. S.; Zoebisch, E. G.; Healy, E. F.; Stewart, J. J. P. AM1: a New General Purpose Mechanical Molecular Model. *J. Am. Chem. Soc.* **1985**, *107*, 3902−3909.
(57) Allen, F. H.; Bellard, S.; Brice, M. D.; Cartwright, B. A.; Doubleday: A.; Higgs, H.; Hummelink, T.; Hummelink-Peters, B. G.; Kennard, O.; Motherwell, W. D. S.; The Cambridge Crystallographic Data Centre: Computer-Based Search, Retrieval, Analysis and Display of Information. *Acta Crystallogr.* **1979**, *B35*, 2331−2339.

(58) (a) Chakravorty, S.; Reynolds, C. H. Improved AMBER torsional parameters for the N−N rotational barrier in diacylhydrazines. *J. Mol. Graph. Model.* **1999**, *17*, 315−324. (b) Günther, R.; Hofmann, H. J. Hydrazino peptides as foldamers: an extension of the beta-peptide concept. *J. Am. Chem. Soc.* **2001**, *123*, 247−255.

(59) (a) DISCOVER, Version 95.0; BIOSYM Technologies, 10065 Barnes Canyon Rd, San Diego, CA 92121. (b) Hagler, A. F.; Lifson, S.; Dauber, P. Consistent force field studies of intermolecular forces in hydrogen-bonded crystals. *J. Am. Chem. Soc.* **1979**, *101*, 5122−5130.

(60) Bogusy, M. J.; Naylor, A. M.; Pitzenberger, S. M.; Nutt, R. F.; Brady, S. F.; Colton, C. D.; Sisko, J. T.; Anderson, P. S.; Veber, D. F. NMR and molecular modeling characterization of RGD containing peptides. *J. Pep. Prot. Res.* **1992**, *39*, 63−76.

(61) Bogdanowich-Knipp, S. J.; Jois, D. S. S.; Siahaan, T. J. The effect of conformation on the solution stability of linear vs cyclic RGD peptides. *J. Pept. Protein Res.* **1999**, *53*, 523−529.

(62) Yamanouchi, J.; Hato, T.; Tamura, T.; Fujita, S. Identification of critical residues for ligand binding in the integrin beta3 I-domain by site-directed mutagenesis. *Thromb. Haemost.* **2002**, *87*, 756−762.

(63) Tozer, E. C.; Liddington, R. C.; Sutcliffe, M. J.; Smeeton, A. H.; Loftus, J. C. Ligand binding to integrin $\alpha_{IIb}\beta_3$ is dependent on a MIDAS-like domain in the beta3 subunit. *J. Biol. Chem.* **1996**, *271*, 21978−21984.

(64) (a) Honda, S.; Tomiyama, Y.; Pampori, N.; Kashiwagi, H.; Kiyoi, T. Kosugi, S.; Tadokoro, S.; Kurata, Y.; Shattil, S. J.; Matsuzawa, Y. Ligand binding to integrin $\alpha_v\beta_3$ requires tyrosine 178 in the α_v subunit. *Blood* **2001**, *97*, 175−182. (b)Yahalom, D.; Wittelsberger, A.; Mierke, D. F.; Rosenblatt, M.; Alexander, J. M.; Chorev, M. Identification of the Principal Binding Site for RGD-Containing Ligands in the $\alpha_v\beta_3$ Integrin: A Photoaffinity Cross-Linking Study. *Biochemistry* **2002**, *41*, 8321−8331.

(65) Hu, D. D.; Barbas, C. F.; Smith, J. W. An allosteric Ca^{2+} binding site on the beta3-integrins that regulates the dissociation rate for RGD ligands. *J. Biol. Chem.* **1996**, *271*, 21745−21751.

(66) Arnaout, M. A.; Goodman, S. L.; Xiong, J. P. Coming to grips with integrin binding to ligands. *Curr. Opin. Cell. Biol.* **2002**, *14*, 641−651.

JM020577M